Research Article ISSN 2639-9466

Nanotechnology & Applications

Flexible Polymeric Films from Starch Reinforced with Graphene Oxide with Microbiological Barrier Properties

Marcello P Santos[1], Karoline C Martins[1], Ana Carolina S Gama[1], Patrick S Ventura[1], Jéssica M Luzardo[1], Alexander M Silva[1], Camila S. de Magalhães[2], Viviane O. de F. Lione[3] and Joyce R Araujo[1]*

[1]Materials Metrology Division, National Institute of Metrology, Quality and Technology (Inmetro), Avenida Nossa Senhora das Graças, 50, Duque de Caxias-RJ, 25250-020, Brazil.

[2]Multidisciplinary Research Center in Computing - Numpex-COMP, Federal University of Rio de Janeiro, UFRJ. Campus Duque de Caxias Professor Geraldo Cidade, Rodovia Washington Luiz, n. 19.593, km 104,5 - Santa Cruz da Serra - Duque de Caxias-RJ, CEP: 25.240-005, Brazil

[3]Pharmaceutical Bioassays Laboratory - LaBioFar, Faculty of Pharmacy, Federal University of Rio de Janeiro, Av. Carlos Chagas Filho, 373 - Cidade Universitária, Rio de Janeiro-RJ, 21941-170, Brazil, Block A, 2nd floor, room 55.

***Correspondence:**
Joyce R Araujo, Materials Metrology Division, National Institute of Metrology, Quality and Technology (Inmetro), Avenida Nossa Senhora das Graças, 50, Duque de Caxias-RJ, 25250-020, Brazil.

Received: 10 Dec 2025; **Accepted:** 11 Jan 2026; **Published:** 22 Jan 2026

Citation: Marcello P Santos, Karoline C Martins, Ana Carolina S Gama, et al. Flexible Polymeric Films from Starch Reinforced with Graphene Oxide with Microbiological Barrier Properties. Nano Tech Appl. 2026; 9(1): 1-10.

ABSTRACT

In order to meet the current environmental demand for sustainable technologies that promote social well-being, the present work consisted of the development of a starch/graphene oxide nanocomposite, suitable for industrial production of disposable packaging fillers. The gelatinized starch films were prepared ultrasonically and after evaporation of the solvent, the specimens were prepared for the following characterizations: chemical, thermal, structural and morphological using Fourier-transform infrared region, X-ray excited photoelectron spectroscopy, thermogravimetry and scanning electron microscopy, respectively. The mechanical properties were evaluated by tensile testing and dynamic-mechanical analysis, while the moisture barrier properties were evaluated by water contact angle and moisture absorption tests using the gravimetric method. The microbiological barrier properties were tested using the Brain Heart Infusion culture medium. The thermogravimetric results indicated higher thermal stability with the incorporation of graphene oxide. Permeability and microbiological barrier studies indicated that, within twenty days of exposure to biological agents in the laboratory environment, the films presented the desired microbiological barrier properties, preventing contamination of the Brain Heart Infusion culture medium. Analyses of nanoscale morphology by scanning electron microscopy showed a significant increase in the roughness of the cross-section fracture surface with increasing graphene oxide content. So, according to the results obtained in relation to mechanical tests, thermal analyses, moisture barrier and microbiological barrier studies, it was observed that graphene oxide, when added to the starch matrix at levels above 0.7 pph, qualifies this material for applications as a moisture blocking layer for multilayer packaging.

Keywords
Starch, Graphene oxide, Barrier properties, Packaging.

Introduction

The industry faces challenges to guarantee the competitiveness of plastic materials regarding cost-benefit in front of more conventional materials such as glass and aluminum, as worldwide, a growing trend has been observed in the search for optimized and intelligent plastic packaging. According to recent data, plastics production from petrochemical sources represents around 70 % of the total market of plastics, while glass and aluminum represent approximately 8 and 4 %, respectively [1]. The prevalence of plastics in human consumption is a result of its versatility and ability to be used in a wide range of industrial applications. Conventional plastics are notable for their strong resistance to chemical products, making them an excellent option to retain

corrosive substances. They are also able to block odors, ensuring the preservation of packaged products [2]. Furthermore, the high transparency of conventional plastics allows food or any other products to be seen inside a package and their low cost makes them economically viable for various uses [3].

The rapid increase in the production and consumption of conventional polymers in recent decades has caused deep environmental impacts globally. These products have changed industrial manufacturing processes in the area of materials engineering and increased the consumption of packaging and everyday materials, enabling economic development and the expansion of consumer markets for products and services. However, with the increase in production and use of plastic materials, atmospheric and water pollution generated due to inadequate disposal and gradual release of microplastics, has become a global ecological emergency for terrestrial and marine ecosystems, posing a risk to human health and biodiversity [4].

Plastics, when discarded in landfills, can take hundreds of years to fully decompose, releasing toxic and harmful compounds into the soil and groundwater. Incineration of plastic waste, although today it is one of the main decomposition methods emits greenhouse gases into the environment, which contribute to air pollution and climate change [5]. According to the guidelines described in ASTM D 883, biodegradable polymers are characterized as polymers that undergo natural decomposition due to the presence of microorganisms in the surrounding environment. This degradation process involves the decomposition of polymers in water, carbon and biomass, which are absorbed by microorganisms and reintegrated into the natural nutrient cycle [6].

There are several types of biodegradable polymers that are being studied to be made viable as a sustainable alternative to conventional plastics. Among them, we can mention polymers based on polyacids, such as polylactic acid (PLA), polymers obtained from renewable sources such as corn, polyhydroxyalkanoates (PHAs), polymers produced by microorganisms through the fermentation of sugars, aliphatic polyesters, such as polybutylenesuccinate (PBS) and, finally, polymers derived from natural sources such as sugar cane and palm oil. Other biodegradable polymers that are also being studied are polymers obtained from potato starch, cassava starch, cornstarch, chitosan, cellulose, among other bio-inputs [7].

Starch combined with graphene oxide (GO) shows promise for packaging applications due to its enhanced barrier and mechanical properties. Studies have been demonstrated that starch/chitosan/GO bionanocomposites have good optical properties, biodegradability and antimicrobial activity, making them suitable for food packaging [8]. According to the work of Zhao et al., the use of GO as a reinforcing agent in starch matrices improves mechanical performance, while reduced graphene oxide (rGO) promotes a significant increase in Young's modulus [9]. In Ferreira et al. [10], the authors affirm that the dispersion of GO in a starch matrix has a positive impact on the biodegradation of these materials. The work of Krystyjan et al. [11] mentioned that the stabilization of suspension of graphene with starch nanoparticles, in the absence of surfactant, resulted in a film with excellent barrier properties to gases and water vapor. In this work, bionanocomposites were prepared from starch reinforced with graphene oxide with the aim of creating flexible, moisture-resistant packaging, which its barrier properties be useful to application in multilayer packaging.

The main objective of this study was to develop and characterize flexible bionanocomposite films based on a starch matrix reinforced with GO to address the inherent mechanical and barrier limitations of pure biopolymers. This work aimed to study the mechanical, thermal, and microbiological barrier properties, as well as the molecular interactions between starch chains and GO through thermogravimetry, mechanical and microbiological barrier tests, FTIR, Raman spectroscopy, and SEM analysis. The incorporation of GO into the starch matrix seeks to ensure prolonged protection of the film against microbiological contamination, thus qualifying the material for active food packaging and innovative applications in multilayer packaging.

Materials and Methods

Samples

The control sample, *i.e.*, pure starch without the reinforcing filler, was prepared from a solution containing 5 g of starch (Sigma-Aldrich - 99,7 %), 40 mL of distilled water, 1.4 mL of glycerol (99.5 %) and 1.2 mL of acetic acid (99.7 %). The precursors were homogenized by magnetic stirring (Corning, PC-420D) for 10 min at a speed of 300 rpm. Subsequently, the film-forming solution was sonicated in an ultrasonic probe tip equipment (Cole Parmer) with an amplitude of 43.2 W for 35 min and kept the temperature below 80 °C. The bionanocomposites were obtained from GO aqueous solutions containing from 0.1 to 1 pph GO, as shown in Table 1. GO fractions were dispersed in 40 mL of distilled water, stirred for 10 min in a vortex equipment and sonicated during 45 min in an ultrasound bath (Ecosonics Ultronique) in order to completely disperse GO nanosheets in aqueous solution. Then, the GO nanosheets solution was added to the solution containing starch, 1.2 mL of acetic acid and 1.4 mL of glycerol under magnetic stirring for 10 min. Next, the mixture was sonicated in an ultrasonic tip for 35 min. Once the film-forming solution was obtained, 30 mL of this solution was pipetted and placed in a 90 mm x 15 mm Petri dish and heated in an oven (Quimis) for 24 h at 40 °C. Finally, the solution in the Petri dish was dried in a desiccator with silica gel, connected to a vacuum pump in order to evacuate the system at a pressure of 53 kPa.

In Figure 1 we can observe the smooth, uniform and bubble-free surfaces of the bionanocomposites films of pure starch and starch containing 0.5 pph and 1.0 pph of GO. Another important aspect observed from Figure 1 was the darkening of the film according with the increase in GO content in the starch matrix. It was also observed that the higher the graphene oxide content, the lower the film contraction.

Figure 1: Images of pure starch and S/GO films containing 0.5 pph and 1.0 pph of GO showing the darkness and the homogeneity of the film surface after GO addition.

Table 1: Starch/GO formulations prepared with different GO contents.

Samples	Starch mass (g)	GO mass (g)
starch	5	0.005
S/GO-0.1%	5	0.010
S/GO-0.2%	5	0.015
S/GO-0.3%	5	0.020
S/GO-0.4%	5	0.025
S/GO-0.5%	5	0.030
S/GO-0.6%	5	0.035
S/GO-0.7%	5	0.040
S/GO-0.8%	5	0.045
S/GO-0.9%	5	0.050
S/GO-1.0%	5	0.005

Chemistry, structure and morphology

Raman spectroscopy analyzes were performed on a Witec Alpha 300 spectrometer with a 514.5 nm laser line using a 100x objective microscope. Laser power was maintained below 0.5 mW to avoid a local heating of the samples. The analyzed spectra were obtained as the average of ten measurements taken at random sample points. At each sample's point, the spectra were acquired using the integration time of 1 s and 10 accumulations in the wavenumber range from 400 cm^{-1} to 1600 cm^{-1}. X-ray diffraction (XRD) data were collected on a D8 Focus Bruker diffractometer using Ni-filtered Cu-Kα radiation (λ = 1.5406 Å) in 2θ range from 5° to 60° with 2θ step of 0.04°. Fourier-transform infrared spectroscopy analyses were performed on a Perkin Elmer Spectrum GX in ATR mode (attenuated total reflectance) with the samples in the form of films and detection range from 400 cm^{-1} to 4000 cm^{-1}. The samples were analyzed by FTIR spectroscopy in the form of films. The chemical composition of the samples were evaluated by X-ray photoelectron spectroscopy (XPS) (ESCAplus P System; Omicron Nanotechnology, Taunusstein, Germany) in an ultra-high vacuum environment (pressure: 10^{-10} mbar), using a non-monochromatic X-ray source, Al anode (Kα = 1486.7 eV), with 20 mA emission current and 15 kV voltage. High-resolution spectra were collected in the C 1s region with 20 eV analyzer pass energy. Scanning electron microscopy (SEM) images were acquired using a FEI SEM Magellan 400 microscope with a field-emission gun (FEG) and in-lens mode. The specimens were prepared by cryogenic fracture and coated with a thin carbon layer (10 nm). The acceleration tension in FEG was 2 kV and the applied current was 0.2 nA. The images were acquired using magnification of 500 x.

Mechanical Characterization

Before mechanical tests, the specimens were dried in a silica gel-containing desiccator kept under vacuum (40 kPa). Therefore, they are removed from the desiccator and placed in an environment for 24 h at 25 (±5) C and 85 (±5) % room humidity before the specimens cutting procedure. The test specimens for the tensile tests were cutted in dumb bell ("tie") format, with dimensions similar to the dimensions of type 3 of the ISO 37 standard. The tensile tests were carried out according to ISO 37:2017 standard in an universal testing machine (Instron, 3365 model), 100 N load cell and 20 mm min^{-1} displacement speed. For each test, 10 specimens were tested. The temperature during the test was 20.60 ± 0.03°C. Dynamic mechanical analysis was carried out on an Instrument DMA SDTA861, Mettler Toledo. The tests were performed by using a compression deformation mode. The specimens were evaluated at 25 °C temperature for 10 min with a maximum amplitude of the force of 20 N and a frequency of 1 Hz (compression mode).

Thermogravimetry (TG)

The thermal stability of the bionanocomposite films were investigated by thermogravimetric analysis cutting their films in order to have a weight of 7 mg. The TG equipment (Gas Controler GC 200 Star System, from TA Instruments) was programmed for heating from 20 °C to 600 °C with a heating rate of 10 °C min^{-1}, under an argon flow of 50 mL min^{-1}. The onset temperature (T_{onset}) is the temperature at which a material begins to exhibit a significant mass change (loss or gain) during a thermogravimetric analysis (T_{onset} in our work was taken as the point of a 3% weight loss).

Moisture absorption and contact angle measurements

Five specimens of each formulation, 2 cm x 2 cm dimensions, were cutted for moisture absorption tests, in agreement with ASTM 5229 standard requirements. Then, the specimens were dried at 50 °C for 48 h (Quimis oven, Q317M-22 model), in order to eliminate moisture before testing. After this process, the specimens were weighed on a precision balance (Bel, HPBG-2285Di model) to determine the specimens initial mass. After initial weighing, the specimens were placed into a desiccator (Dry-Box, DVC 3200 model), with 87 % of humidity, for the absorption moisture

evaluation. Subsequent weighing occurred every 30 min and were maintained until 15 h of experiment, as during this interval, saturation behavior was reached. For statistical data analysis, the collected values were submitted to a Tukey test.

Biological assays

Microbial permeability assay

In order to investigate the ability of the starch/GO bionanocomposites to prevent microbial penetration, microbiological tests were conducted based on the method cited by Souza, C.S.d, et al. Test tubes containing 3 ml of sterile brain heart infusion medium (BHI; Sigma–Aldrich) were sealed with a 3 cm^2 size film at aseptic conditions. Positive and negative controls were prepared in an open and a completely sealed test tube, respectively. The assembly was placed in an open environment and the progress of microbial permeation was observed for 20 days. The cloudiness of the medium in any test tube was recorded as microbial contamination. Two independent experiments were performed in duplicate.

Results and Discussion

Bulk and surface molecular structure of starch-GO films

Figure 2a presents the FTIR spectrum of pure starch samples and starch films containing representative concentrations of GO, where it is possible to observe the main characteristic bands corresponding to the vibrational modes of the chemical bonds present in the molecular structure of starch, as well as graphene oxide filler. The intensity and position of the starch bands change as the concentration of GO increases, indicating molecular chemical interactions between starch and GO and, consequently, in the thermal, mechanical, morphological and structural properties of the bionanocomposite films.

Table 2 compiles the main bands observed in the FTIR spectra presented in Figure 2a, as: a broad band around 3300 cm^{-1} assigned as the stretching of the O-H bonds, corresponding to the hydroxyl groups (C-OH) of starch. The broad and intense peak from 3000 cm^{-1} to 3600 cm^{-1} in the GO FTIR spectrum may be attributed to hydroxyl groups and intercalated H_2O molecules between the GO flakes [12]. As discussed by Acik et al. [12], the FTIR spectrum of GO, prepared by oxidation of the graphite powder according to a modified Hummer's method [13], shows a free hydroxyl band between 3000 cm^{-1} and 3700 cm^{-1} and another band at 3550 cm^{-1} from OH in carboxylic group. The band at 3200 cm^{-1} was assigned as OH from adsorbed water molecules (14). The GO FTIR spectrum shows a main band at 3409 cm^{-1} (from hydroxyl groups on both the basal plane and the edge) and two shoulders at 3223 cm^{-1} (from adsorbed water molecules) and 3590 cm^{-1} (carboxyl groups), which are consistent with the literature assigned peaks for multilayer GO and OH from adsorbed water. In the GO/starch FTIR spectra, a main band at 3305 cm^{-1} was observed related to the OH stretching vibration of amylopectin and amylose chains [15,16].

Although it has been reported in the literature a blue shift of the stretching frequency of -OH from carboxyl groups in the FTIR spectrum of the S/GO bionanocomposites [16,17], we may not infer this behavior in the present work due to the small GO concentration in the S/GO films. In contrast, another study reported [15] a blue shift in OH stretching when an S/GO nanocomposite was prepared in the proportion 1:1.

The peaks near 2930 cm^{-1} are typical of C-H stretching vibrations, whereas the bands at 1641 cm^{-1} and 1410 cm^{-1} are assigned to the δ (O-H) bending of water and CH_2, respectively. The band at 997 cm^{-1} was attributed to the stretching vibration of C-O in the C-O-C groups. The band at 1156 cm^{-1} is related to the axial strain vibrations of the C − O groups in alcohols and C − O − C (C - O - C asymmetric stretching) [18]. The presence of this band in all spectra indicates that the basic structure of starch is maintained even with the addition of GO. This result is promising considering that Khurshida et al. [19] reported that the interaction between ST and GO might induce changes in the starch structure, such as the formation of complexes or the disruption of the starch helix. These changes may affect film properties, such as stiffness, mechanical strength and permeability [19,20], which was not evidenced in the present study.

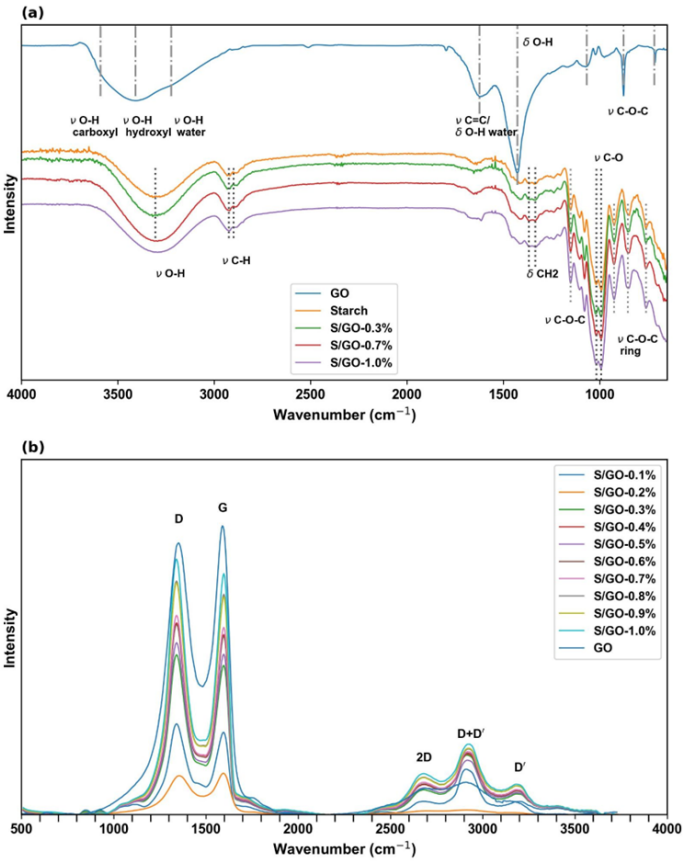

Figure 2: (a) FTIR spectra of starch and bionanocomposites S/GO-0.3%, S/GO-0.7%, and S/GO-1.0% samples. (b) Raman spectra of all formulations of the bionanocomposites from starch and GO.

Figure 2b shows Raman spectra for all formulations of the ST/GO bionanocomposites, as well as for GO by itself. The spectrum of pure GO exhibits two main bands, centered at 1594 cm^{-1} and

1348 cm^{-1}, assigned as G and D bands, respectively. The first one, the G-band, represents the E_{2g} vibrational mode of crystalline graphite, and the D-band is associated to A_{1g} breathing mode due to structural disorder [21]. As a second order of the D-band, the graphene Raman spectra show the 2D-band, centered at about 2700 cm^{-1}, typically assigned as an overtone of the D-band [22]. Besides the 2D-band, other bands could appear in the multilayered GO Raman spectrum [23] as the D+D' and 2D' bands in the region ranging from 2800 cm^{-1} to 3300 cm^{-1}. D+D' band, centered at about 2900 cm^{-1}, is a combination of D and D'-band and the 2D'-band, centered at about 3200 cm^{-1}, does not coincide with other modes being observed, even without defects. All these bands are assigned as graphene structures according to literature [24-27].

Raman spectra of the S/GO bionanocomposites only feature bands regarding GO vibrational modes. Table 3 shows the parameters calculated from the deconvolution of Raman spectra with Lorentzian function. An increase in the area of the D band and G band was observed as the GO content increases, which is expected, since the area of these bands is directly proportional to the concentration of the species. From the results shown in Tab. 2, is possible to observe that $A_D/A_G = 1.86$ for pure GO sample, while AD/AG ranged from 1.66 to 1.77 for S/GO bionanocomposite samples, that is, GO nanosheets, when dispersed in the starch matrix, showed a lower concentration of defects than the isolated GO nanosheets. In the literature, there are some works [15,17] reporting that carbohydrates act as a partial reducing agent of graphene oxide reducing the labile oxygenated carbon groups of the basal plane of GO being a possible explanation for the A_D/A_G reduction in the S/GO nanocomposites.

Thermogravimetry (TG)

The results of TG are summarized in Figure 3. It was observed the main characteristic weight loss process for different formulations of ST/GO bionanocomposite. The first weight loss process is related to the desorption of water molecules [17]. We can observe an increase in T_{onset} values as GO content increases in S/GO formulations, Table 3. The temperature increase occurs because the continuous addition of GO will demand more thermal energy for the removal of water molecules trapped inside GO layers [27].

The influence of GO on the thermal stability of starch biopolymers is evidenced by the increase of the maximum temperature, $T_{máx}$, of the bionanocomposites. Figure 3a shows thermal decomposition ($T_{máx}$) of pure starch centered at 315 °C, typically assigned as a thermal decomposition of amylose and amylopectin [28]. In relation to the pure starch, the S/GO bionanocomposites did not show a significant temperature increase, indicating that GO does not change the thermal stabilization of the starch matrix.

In Table 4, it is observed that the residue obtained after thermal degradation does not change in formulations with 0.3 pph and 0.5 pph of GO, when compared to pure starch. In the other hand, a slight increase in the residue content in the formulation with 1.0 pph of GO was observed in formulations with a higher GO content (1.0 pph). This result is an indicative that GO, at higher

Table 2: FTIR band assignment of starch and S/GO bionanocomposites.

Literature	Functional groups	Starch	GO	S/GO-0.3%	S/GO-0.7%	S/GO-1.0%
3600 – 3300	O - H stretching (C-OH, COOH, H_2O)	3319	3230	3319	3293	3292
2931	C - H stretching	2922	2890	2922	2922	2922
1637	C-O bending associated with OH group	1637		1637	1638	1637
1458	CH2 symmetric deformation	1463		1463	1463	1463
1415	CH2 symmetric scissoring	1417		1417	1417	1417
1385-1375	C -H symmetric bending	1367	1334	1367	1367	1367
1149	C - O - C asymmetric stretching	1151		1151	1151	1151
1200 – 800	C - O stretching	1017	993	1017	1017	1017
920, 856, 758	C - O - C ring vibration of carbohydrate	925 853 759		925 853 759	925 853 759	925 853 759

Table 3: Spectroscopic parameters of experimentally observed Raman D-band and G-band of S/GO bionanocomposites.

Samples	A_D	A_G	$FWHM_D$	$FWHM_G$	ω_D	ω_G	A_D/A_G	I_D/I_G
GO	384986	206624	176.67	94.04	1352.74	1584.63	1.86	0.99
S/GO-0.1%	78344	44203	120.05	74.07	1340.90	1595.51	1.77	1.09
S/GO-0.2%	109979	62420	120.28	72.59	1337.44	1592.50	1.76	1.06
S/GO-0.3%	135579	79752	116.47	72.86	1340.87	1595.64	1.69	1.06
S/GO-0.4%	162130	96216	115.59	72.52	1340.88	1595.68	1.69	1.06
S/GO-0.5%	146786	86484	116.69	72.87	1340.87	1592.54	1.69	1.06
S/GO-0.6%	160754	95524	115.30	72.16	1340.86	1592.65	1.68	1.05
S/GO-0.7%	166366	99940	113.95	72.07	1340.87	1592.69	1.67	1.05
S/GO-0.8%	194989	115374	114.18	70.60	1337.37	1592.72	1.69	1.05
S/GO-0.9%	190691	114554	112.19	71.10	1340.77	1595.77	1.66	1.06
S/GO-1.0%	211655	125667	113.17	70.25	1337.29	1592.83	1.68	1.05

concentrations, may act as a protective agent against thermal degradation, probably due to its robust structure and ability to form a denser network within the starch matrix, and consequently, increasing the resistance of the material to thermal degradation [29].

Table 4: Thermogravimetric data of pure S and S/GO bionanocomposites showing T_{onset}, T_{max} and residue percentage at 600 °C.

Samples	T_{onset} (°C)	T_{max} (°C)	Residue at 600 °C (%)
S	107.46	315.46	9.39
S/GO-0.3%	124.95	326.67	7.38
S/GO-0.5%	124.62	326.25	8.22
S/GO-1.0%	146.65	321.71	16.13

GO promotes also enhanced thermal stability, indicated by the shifts on T_{onset} and T_{max} *values* in the S/GO formulations. This effect suggests a transition behavior depending on the GO content be enough to allow the formation of a percolation network connecting the GO nanoparticles that at these levels, may act as a protective barrier, which enhances resistance to the thermal degradation [29].

Moisture absorption

Figure 4 illustrates the moisture content of pure starch and S/GO bionanocomposites over 15 h at 23 °C. A fast increasing in moisture content is observed during the first 4 h, driven by the saturation of active sites of the film due to the presence of water at the onset of the process [30]. This initial stage represents the early water sorption phase of the films. The pure starch exhibits a slight higher water absorption rate than the bionanocomposites film. This behavior may be attributed to the presence of amylose and amylopectin, which contain OH functional groups at the surface, which favors water diffusion throughout the starch matrix [31].

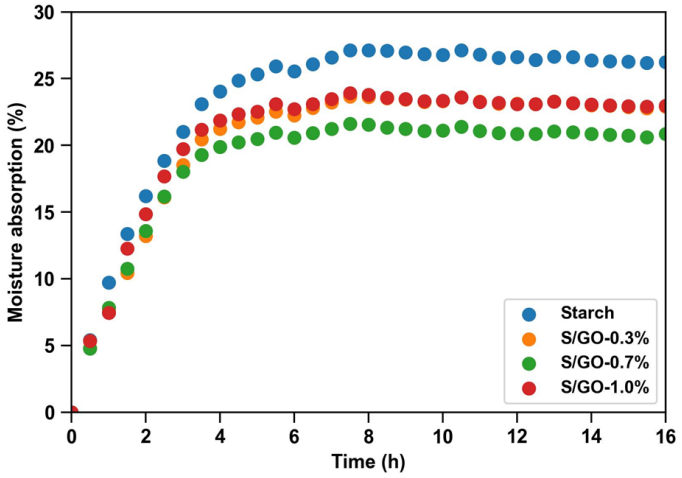

Figure 4: Moisture absorption curves of pure S and S/GO bionanocomposites, at 23 °C temperature and 80% relative humidity, showing the moisture absorption kinetic, saturation behavior comparing the different formulations.

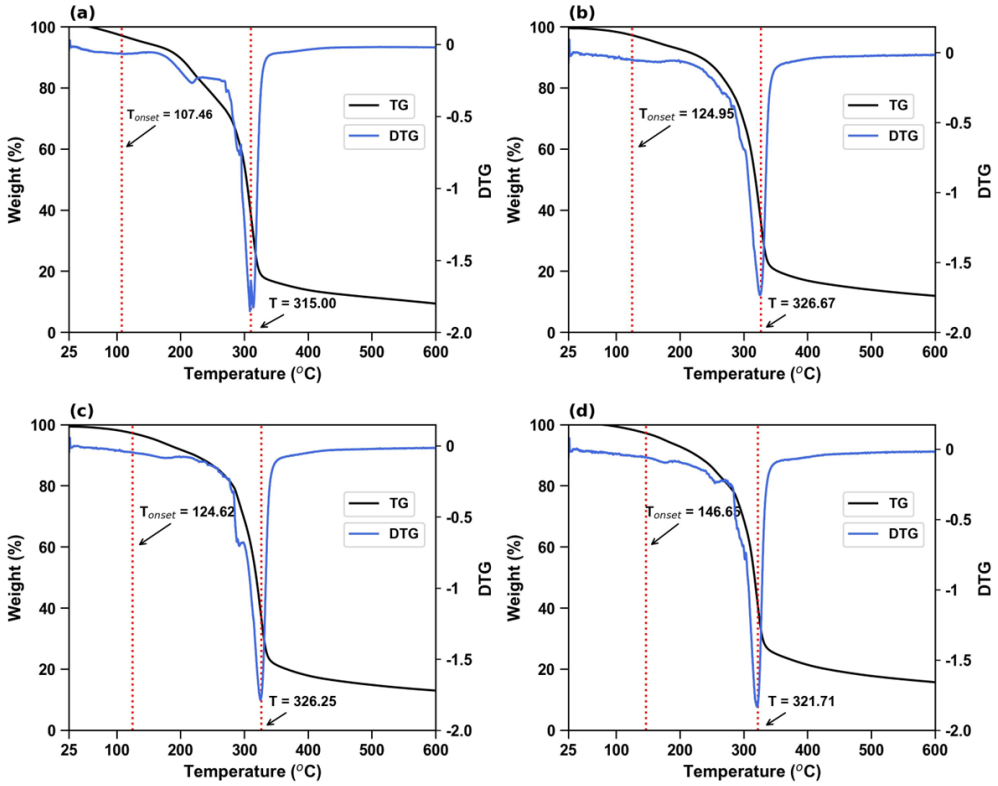

Figure 3: Weight loss thermogravimetric curves and first derivative of weight loss vs. temperature plot for (a) starch, (b) S/GO-0.3%, (c) S/GO-0.5%, (d) S/GO-1.0% samples showing the thermal degradation process of S and S/GO films.

Statistical analysis of moisture absorption data showed that S/GO-0.7% bionanocomposite reached water saturation sooner than the S/GO-0.3% and S/GO-1.0% samples. However, the total water absorption capacity of the S/GO-0.7% formulation, as derived from the values in Figure 4, was found to be significantly lower than the S/GO-0.3%, S/GO-1.0% formulations, and pure starch. The behavior of the S/GO-0.7% sample may be explained by the structural properties and, specifically, the pore size distribution within the bionanocomposites. It appears that the S/GO-0.7% composite exhibits a considerably reduced average pore diameter compared to the other samples and the pure starch control. This apparent pore size reduction is likely the result of more effective interactions between the amylose/amylopectin chains and the GO nanoparticles, which promotes a denser polymer network and consequently, decrease in the pore size [32].

Mechanical properties

Tensile tests

The effect of GO content on the mechanical properties of the bionanocomposites is presented in Figure 5. The Young's modulus (E'), tensile strength (σ_b) and elongation at break exhibit non-linear trends as GO content increases. Concerning GO contents up to 1.0 pph, the E' increased from 17.1 MPa to 23.4 MPa, reaching a maximum of 49.0 MPa at 0.7 pph of GO (Figure 5a). However, the values for 0.3 pph and 0.5 pph concentrations were statistically similar to pure starch. Similarly, σ_b increased with the increase in GO concentration, reaching the maximum at 0.5 pph of GO (Figure 5b). In contrast, elongation at break typically decreases as GO content increases—attributed to restricted polymer chain flow—with exception of the 0.7 pph GO formulation, which showed a significant increase to 112 % (Figure 5c). The observations are in agreement with previous studies [33,34]. The overall enhancements in E' and σ_b are attributed to strong interfacial interactions and effective dispersion of GO within the starch matrix. The improved performance of the S/GO-0.7% formulation suggests a percolation network formation from this GO content, resulting in superior mechanical reinforcement.

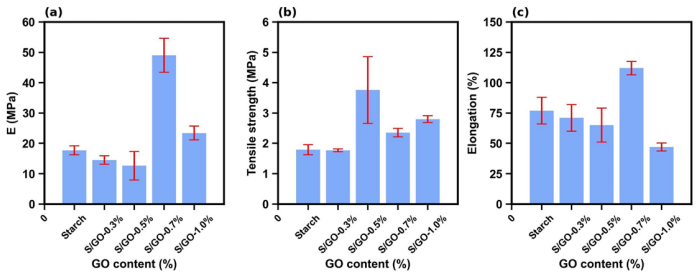

Figure 5: (a) The Young's modulus (E'), (b) tensile strength (σ_b) and (c) elongation at break tests of pure starch and S/GO samples.

Dynamic Mechanical Analysis

The viscoelastic properties of the S/GO bionanocomposites were evaluated using DMA. Figure 6 illustrates the evolution of the storage modulus (E') and the damping factor (tan δ) as a function of GO concentration.

As demonstrated in the profiles, the integration of GO nanoflakes resulted in a substantial enhancement of the storage modulus across the analyzed temperature range. The most remarkable reinforcement was observed in the S/GO-0.7% formulation, which yielded an E' value of 54.3 MPa. For comparative purposes, this represents an approximate four-fold increase over the storage modulus of the neat starch control (13.6 MPa), highlighting the high efficiency of GO as a reinforcing agent.

These DMA findings correlate strongly with the previously discussed tensile data; the incorporation of GO simultaneously improves both the stiffness (E') and tensile strength (σ_b) of the bionanocomposites. This mechanical synergy may be attributed to the superior dispersion of the nanofiller within the polymeric matrix and the robust interfacial interactions—specifically hydrogen bonding and polar attractions—between the GO oxygenated groups and the starch chains [31,32]. These interactions effectively restrict the segmental mobility of the polymer chains, thereby enhancing the material's ability to store elastic energy and resulting in a more structurally rigid and resilient composite network.

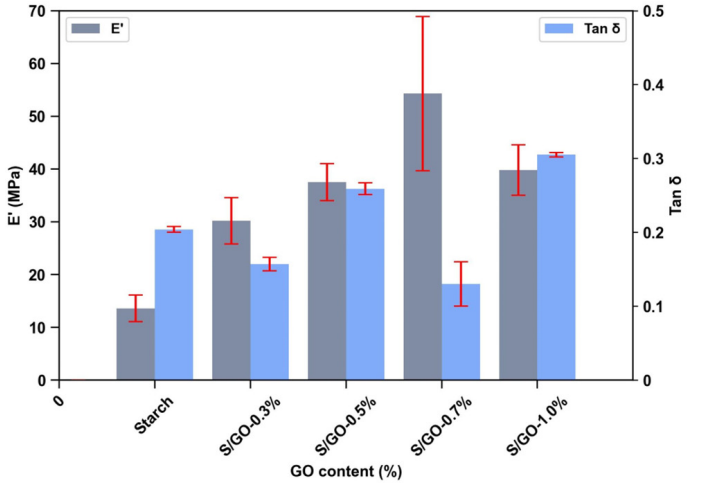

Figure 6: DMA analysis of pure starch and S/GO samples.

Morphology analysis by scanning electron microscopy (SEM)

The micrographs presented in Figure 7 illustrate the morphological evolution of pure starch films compared to S/GO formulations at concentrations of 0.3 pph, 0.5 pph, 0.7 pph and 1.0 pph of GO. Analysis of the pure starch film (Figure 7a) reveals a characteristic porosity on the cryofracture surface. The introduction of GO into the starch matrix resulted in an increased surface roughness as the GO content increase.

Comparing the different samples, the neat starch sample SEM image (Figure 7a) and the 0.3 pph GO sample image (Figure 7b) show a flat surface with small imperfections probably related to the cryofracture process [35]. On the other hand, from 0.5 pph of GO, it is possible to observe the GO presence in the form of wrinkles and flakes on the surface (Figure 7c - Figure 7e) [36]. These surface heterogeneities are critical, as surface topography

directly influences mechanical strength, permeability, and optical properties [37]. Furthermore, the balance between porosity and roughness is a key determinant for the material's biocompatibility in advanced applications [38].

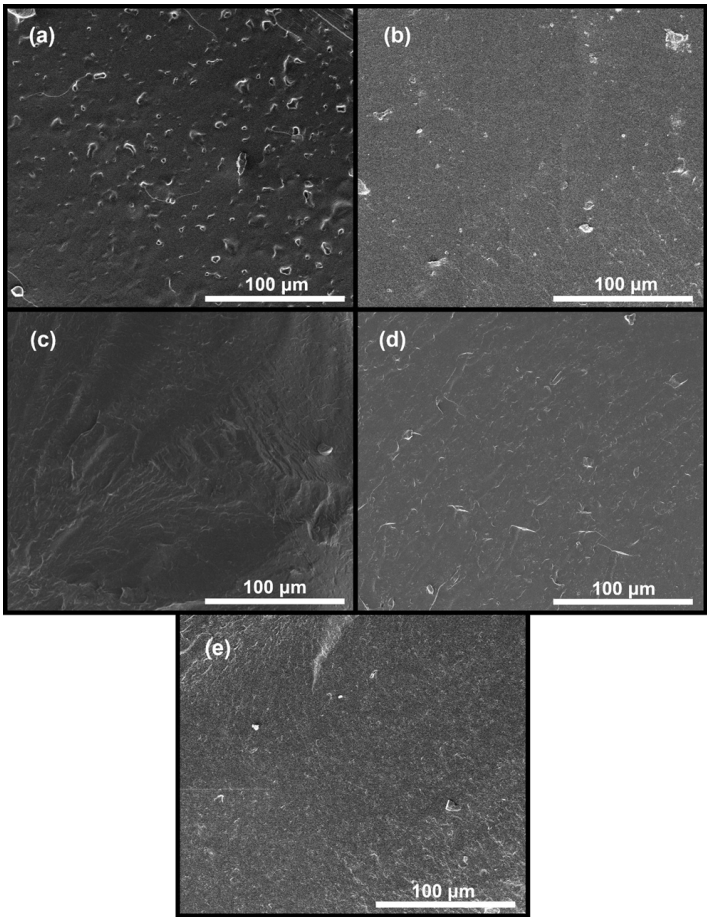

Figure 7: Morphology of starch and starch/GO bionanocomposite. SEM images of (a) starch, (b) S/GO-0.3%, (c) S/GO-0.5%, (d) S/GO-0.7%, and (e) S/GO-1.0% samples.

Microbial permeability assay

The effectiveness of the developed films in preventing microbial infiltration was rigorously evaluated using BHI culture medium. Sealed tubes were monitored over a 20-day incubation period, with specific observations conducted on days 1, 7, and 20 days, as illustrated in Figure 8.

Throughout the entire experimental timeframe, all tubes sealed with the various film formulations maintained complete medium transparency. The absence of turbidity—a primary indicator of microbial proliferation—confirms that no bacterial infiltration occurred. These results demonstrate that the films, regardless of their specific chemical composition or GO content, act as a highly effective microbiological barrier [39].

The consistent stability of the BHI medium underscores the material's structural integrity and its efficacy as a robust microbiological shield, highlighting its potential for use in sterile packaging or biomedical applications where long-term contamination prevention is critical [40].

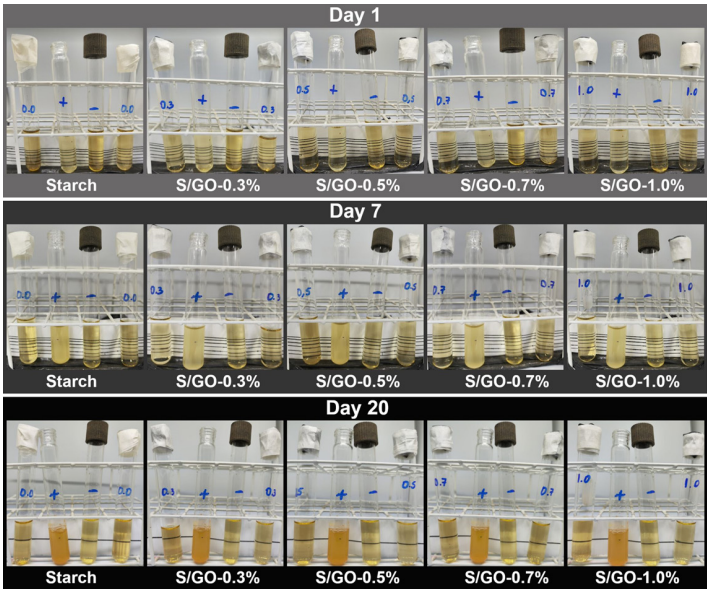

Figure 8: Monitoring of the pure starch specimens and starch with 0.3 pph, 0.5 pph, 0.7 pph, and 1.0 pph of GO after 1, 7 and 20 days of exposure to the environment

Conclusion

Graphene oxide incorporation into the starch matrix proved to be an effective strategy for modulating the physicochemical and functional properties of the material aiming packaging applications. FTIR analysis revealed synergic molecular chemical interactions between starch matrix with GO. These interactions are crucial for the integration of GO into the polymeric matrix and for the consequent improvement of the materials macroscopic properties.

From the perspective of thermal stability, TG analysis result indicated an increase in the thermal stability of the bionanocomposites with the incorporation of GO. At higher concentrations, GO appears to act as a protective agent against total degradation, likely due to its robust structure and the formation of a dense percolation network within the starch matrix, up to 0.5 pph of GO content, which restricts the mobility of polymer chains and retards thermal decomposition.

Barrier properties were significantly enhanced with GO addition and moisture absorption tests demonstrated a reduction in moisture retention with increasing GO content, indicating an improvement in the moisture barrier. SEM morphological analysis revealed an increase in the roughness of the fracture surface with increasing GO. This more compact morphology directly contributes to the improved barrier properties, hindering the permeation of water molecules and microorganisms.

Therefore, the films exhibited desired microbiological barrier properties, preventing contamination of the culture medium for a period of twenty days. This behavior is of paramount importance

for food packaging applications, where protection against microbial degradation is essential for product safety and shelf life.

Therefore, this study demonstrates that the addition of graphene oxide to the starch matrix, especially at levels around 0.7 pph, provides the reinforcement effect of polymeric films with a combination of higher thermal stability, improved moisture barrier, and consequently, effective microbiological protection.

These characteristics qualify the material for innovative applications as protective layers in multilayer packaging, offering a promising solution for the development of more sustainable packaging with enhanced performance.

References

1. Tilsted JP, Bauer F, Birkbeck CD, et al. Ending fossil-based growth: Confronting the political economy of petrochemical plastics. One Earth. 2023; 6: 607-619.
2. Zheng K, Wu Y, Hu Z, et al. Progress and perspective for conversion of plastic wastes into valuable chemicals. Chem. Soc. Rev. 2023; 52: 8-29.
3. Jambeck J, Walker-Franklin I. The impacts of plastics' life cycle. One Earth. 2023; 6: 600-606.
4. Hoang TC. Plastic pollution: Where are we regarding research and risk assessment in support of management and regulation? IEAM. 2022; 18: 851-852.
5. Wu Y, Chen X, Liu Q, et al. Informal landfill contributes to the pollution of microplastics in the surrounding environment. Environ. Pollut. 2021: 293: 118586.
6. Dallaev R, Papez N, Allham MM, et al. Biodegradable Polymers: Properties, Applications, and Environmental Impact. Polymers. 2025; 17: 1981.
7. Arruda TR, Machado GO, Marques CS, et al. An Overview of Starch-Based Materials for Sustainable Food Packaging: Recent Advances, Limitations, and Perspectives. Macrmol. 2025; 5: 19.
8. Dutta D, Sit N. Comprehensive review on developments in starch-based films along with active ingredients for sustainable food packaging. Sustain. Chem. Pharm. 2024; 39: 101534.
9. Zhao W, Sugunan A, Gillgren T, et al. Surfactant-free starch-graphene composite films as simultaneous oxygen and water vapour barriers. npj 2D Mater. Appl. 2022; 6: 1-9.
10. Ferreira WH, Andrade CT. Physical and biodegradation properties of graphene derivatives/thermoplastic starch composites. Polysaccharides. 2021; 2: 582-593.
11. Krystyjan M, Khachatryan G, Grabacka M, et al. Physicochemical, Bacteriostatic, and Biological Properties of Starch/Chitosan Polymer Composites Modified by Graphene Oxide, Designed as New Bionanomaterials. Polymers. 2021; 13: 2327.
12. Acik M, Lee G, Mattevi C, et al. The Role of Oxygen during Thermal Reduction of Graphene Oxide Studied by Infrared Absorption Spectroscopy. J. Phys. Chem. 2011; 115: 19761-19781.
13. Hummers Jr WS, Offeman RE. Preparation of Graphitic Oxide. JACS 1958; 80: 1339-1339.
14. Hontoria-Lucas C, Lopez-Peinado AJ, Lopez-Gonzalez J, et al. Study of oxygen-containing groups in a series of graphite oxides: Physical and chemical characterizatio. Carbon. 1995; 33: 1585-1592.
15. Rapisarda M, Marken F, Meo M, et al. Graphene oxide and starch gel as a hybrid binder for environmentally friendly high-performance supercapacitors. Commun Chem. 2021; 4: 169.
16. Xu H, Xie L, Wu D, et al. Immobilized graphene oxide nanosheets as thin but strong nanointerfaces in biocomposites. ACS Sustainable Chem. Eng. 2016: 4: 2211-2222.
17. Peregrino PP, Sales MJA, Silva MFP, et al. Thermal and electrical properties of starch–graphene oxide nanocomposites improved by photochemical treatment. Carbohydr Polym. 2014; 106: 305-311.
18. Abdullah AHD, Chalimah S, Primadona I, et al. Physical and chemical properties of corn, cassava, and potato starchs. IOP Conf. Ser.: Earth Environ. Sci. 2018; 160: 012003.
19. Khurshida S, Das MJ, Sankar C Deka, et al. Effect of dual modification sequence on physicochemical, pasting, rheological and digestibility properties of cassava starch modified by acetic acid and ultrasound, Int. J. Biol. Macromol 2021; 188: 649-656,
20. Lima BN, Cabral TB, Neto RP, et al. Estudo do amido de farinhas comerciais comestíveis. Polímeros. 2012; 22: 486-490.
21. Tuinsta F, Koenig JL. Raman spectrum of graphite. J. Chem. Phys. 1970; 53: 1126-1130.
22. Ferrari AC, Meyer JC. Scardaci V, et al. Raman spectrum of graphene and graphene layers. Phys. Rev. Lett. 2006; 97: 187401.
23. Charlier, JC, Eklund PC, Zhu J, et al. Electron and Phonon Properties of Graphene: Their Relationship with Carbon Nanotubes. In: ed. Carbon Nanotubes. Topics Appl Physics. 2011; 111.
24. Saito R, Hofmann M, Dresselhaus G, et al. Raman spectroscopy of graphene and carbon nanotubes. Adv. Phys. 2011; 60: 413-550.
25. Ribeiro-Soares J, Oliveros ME, Garin C, et al. Structural analysis of polycrystalline graphene systems by Raman spectroscopy. Carbon. 2015; 95: 646-652.
26. Kaniyoor A, Ramaprabhu SA. Raman spectroscopic investigation of graphite oxide derived graphene. AIP Adv. 2012; 2: 032183.
27. Qiu Y, Guo F, Hurt R, et al. Explosive thermal reduction of graphene oxide-based materials: mechanism and safety implications. Carbon. 2014; 72: 215-223.
28. Malucelli LC, Lacerda LG, Carvalho MAS, et al. Porous waxy maize starch: thermal, structural and viscographic properties of modified granules obtained by enzyme treatment. J. Therm. Anal. Calorim. 2015; 120: 525-532.

29. Baishya P, Maji TK. A comparative study on the properties of graphene oxide and activated carbon based sustainable wood starch composites. Int. J. Bio. Macromol. 2018: 115: 970-977.
30. Chinma CE, Ariahu CC, Alakali JS, et al. Effect of temperature and relative humidity on the water vapour permeability and mechanical properties of cassava starch and soy protein concentrate based edible films. J. Food Sci. Technol. 2015; 52: 2380-2386.
31. Liu R, Gong T, Zhong K, et al. Graphene oxide papers with high water adsorption capacity for air dehumidification. Sci. Rep. 2017; 7: 9761.
32. Bai Z, Wang T, Zheng X, et al. High strength and bioactivity polyvinyl alcohol/collagen composite hydrogel with tannic acid as cross-linker. Polym. Eng. Sci. 2021; 61: 278-287.
33. Li R, Liu C, Ma J, et al. Studies on the properties of graphene oxide-reinforced starch biocomposites. Carbohydr. Polym. 2011; 84: 631-637.
34. González K, Larraza I, Martin L, et al. Effective reinforcement of plasticized starch by the incorporation of graphene, graphene oxide and reduced graphene oxide. Int. J. Biol. Macromolecules. 2023; 249: 126130.
35. Żołek-Tryznowska Z, Bednarczyk E, Tryznowski M, et al. A comparative investigation of the surface properties of corn-starch-microfibrillated cellulose composite films. Materials. 2023; 16: 3320.
36. Cahyana Y, Verrell C, Kriswanda D, et al. Properties comparison of oxidized and heat moisture treated (hmt) starch-based biodegradable films. Polymers. 2023; 15: 2046.
37. Podgorbunskikh E, Kuskov T, Matveeva A, et al. Disordering of starch films as a factor influencing the release rate of biologically active substances. Polymers. 2023; 15: 2303.
38. Velásquez-Castillo LE, Leite MA, Tisnado VJA, et al. Cassava starch films containing quinoa starch nanocrystals: Physical and surface properties. Foods. 2023; 12: 576.
39. Liu Z, Liu X. Enhanced Antibacterial Performance of Chitosan/Corn Starch Films Containing TiO_2/Graphene for Food Packaging. Polymers. 2022; 14: 3844.
40. Huang Y, Yao Q, Wang R, et al. Development of starch-based films with enhanced hydrophobicity and antimicrobial activity by incorporating alkyl ketene dimers and chitosan for mango preservation. Food. Chem. 2025; 467: 142314.
41. Souza C.S.d., Lopes V.R.d.C., Barcellos G, et al. Unleashing Fungicidal Forces: Exploring the Synergistic Power of Amphotericin B-Loaded Nanoparticles and Monoclonal Antibodies. J. Fungi. 2024; 10: 344.